García-Pozuelo, D., Olatunbosun, O., Strano, S., Terzo, M. (2019). A real-time physical model for strain-based intelligent tires. *Sensors and Actuators A: Physical*, 288, pp. 1-19.

DOI: https://doi.org/10.1016/j.sna.2018.12.010

A real-time physical model for strain-based intelligent tires

Daniel Garcia-Pozuelo[1], Oluremi Olatunbosun[2], Salvatore Strano[3*], Mario Terzo[3]

[1]*Mechanical Engineering Department, Universidad Carlos III de Madrid, 28911 Madrid, Spain.*

[2]*School of Mechanical Engineering, University of Birmingham, Edgbaston B15 2TT, UK.*

[3]*Department of Industrial Engineering, University of Naples Federico II, 80125 Naples, Italy.*

[*]*corresponding author: salvatore.strano@unina.it*

Abstract

In recent years, a large amount of research has been focused on intelligent tire technology. Several systems have been developed based on different sensors installed on tires. Nowadays one of the major research problems for intelligent tire development is how to correlate measurements provided by sensors to the tire dynamics. The methods mostly presented in literature are based on empirical correlations between measurements and tire working conditions obtained with extensive experimental activities which are expensive and time consuming.

In this paper, a real-time physical model suitable to describe the longitudinal dynamics of strain-based intelligent tires is described. The mathematical tire model consists of a flexible ring on a viscoelastic foundation. The solution of the model dynamics has been obtained in closed form and the model parameters have been identified from experimental data. The comparison between the simulated strains and the ones provided by an intelligent tire prototype highlighted that the proposed tire model can estimate with an acceptable precision the tire deformations for several operative working conditions.

keywords: intelligent tire; flexible ring model; real-time tire model; tire strain.

1. Introduction

The identification of driving conditions from tires is of crucial importance for safety, performance and stability of vehicles. Therefore, in the last decades, considerable research effort has been focused on the development of intelligent tires that are able to provide useful information about tire and road conditions. For instance, intelligent tire concept can be adopted for estimating forces at the tire-road interface, tire wear, contact patch length, friction coefficient, slip angle and road conditions [1]. A sensor system inside an intelligent tire could improve driving safety by sending reliable data to drivers via vehicle-to-vehicle or via vehicle-to-infrastructure communications [2]. Moreover, intelligent tires could be able to interact with different vehicle control systems, such as Anti-lock Braking System (ABS), Electronic Stability Control (ESC), Traction Control System (TCS), Suspension Control System (SCS).

Research on intelligent tires began with the development of the tire pressure monitoring system (TPMS) that warns the driver if a tire is significantly under-inflated. More recently, different types of intelligent tire concepts have been proposed. Most of them are based on accelerometers or strain sensors attached to the inner liner of the tire on the tread portion [3].

In [4], real-time acceleration measurements have been adopted for estimating several parameters of the tire and the road conditions. Negrus *et al.* [5] presented experimental results concerning an intelligent tire equipped with acceleration sensors and a wireless data transmission system.

An algorithm for contact patch determination and friction coefficient estimation based on radial and lateral acceleration profiles has been presented in [6]. The compact size of accelerometers together with their inexpensive cost make them suitable for intelligent tires in the market [7]. However, as mentioned in APOLLO project [8], accelerations are very sensitive to noise from the road interaction and consequently sophisticated signal processing procedures are required for extracting tire characteristics. As claimed in the APOLLO project [8], strain sensors in intelligent tire applications outperform accelerometers for wheel force estimation. Strain measurements are not affected by the tire rotational speed and the noise level is generally lower than the one of accelerometers. In addition, strain sensors are less expensive than other sensors, reliable and accurate enough to measure strain data under dynamic conditions.

Several types of strain sensors have been developed based on different measuring principles. Polyvinylidene fluoride (PVDF) strain sensors, attached to the inner liner have been adopted in [9, 10] in order to measure tread ring deformations. A Surface Acoustic Wave (SAW) device has been used in [11] for measurement of tread deformation for friction estimation.

In [12], the tread ring strain has been obtained from the capacitance variation of an oscillating circuit integrated with the tire. In [13], the tread deformation has been obtained from a magnetic sensor. Magnetic sensors for sidewall strain measurements have been also adopted in [14] for wheel force estimation. Optical fiber sensors have been employed in [15, 16] for inner liner strain measurements. In [17], a fuzzy logic algorithm, for the estimation of slip angle and tire working conditions from strain measurements, has been presented.

The developments of the above mentioned intelligent tire concepts require time-consuming process due to extensive experiments necessary to correlate sensor measurements with the tire operative conditions. To overcome this limitation, mathematical modelling of intelligent tires for simulation tests could be of vital importance. Moreover, real-time models could be implemented in observers for tire condition estimations from strain measurements.

Conventional tire models are not suitable for modelling strains in intelligent tires because they provide as output forces starting from longitudinal and lateral slips, frictions, etc. [18-23]. For instance, the magic formula tire model developed by Pacejka gives tire forces based on regression equations related to experimental data [24, 25]. Finite element tire models are often used for determining tire strains but they are not suitable for real-time applications due to their computational loads [26].

In this paper, a tire strain model is presented. The proposed model can predict, in real-time, the tire strain according to the driving conditions. More specifically, the physical modelling approach is based on the tire flexible ring model which provides deformations of the tire carcass due to applied steady-state in-plane forces [27]. The model has been validated through experimental data from an intelligent tire presented in [1, 17]. The experiments have been carried out by means of strain sensors inserted on the tire inner liner and an indoor tire test rig.

This paper is organized as follows: in section 2, the intelligent tire system considered for the model validation is briefly introduced. The proposed tire model is presented in section 3 and its experimental validation is described in section 4. Conclusions and future developments are drawn in section 5.

2. Outline of the strain-based intelligent tire

A strain-based intelligent tire prototype, developed in the Vehicle Dynamics Laboratory at the University of Birmingham, has been considered in this study [28]. It is a Dunlop slick radial tire 175/505 R13 for SAE Formula Student, shown in Fig. 1a. The 175/505 R13 radial tire consists of

different rubber components with embedded reinforcements as illustrated in the tire cross section reported in Fig. 1b.

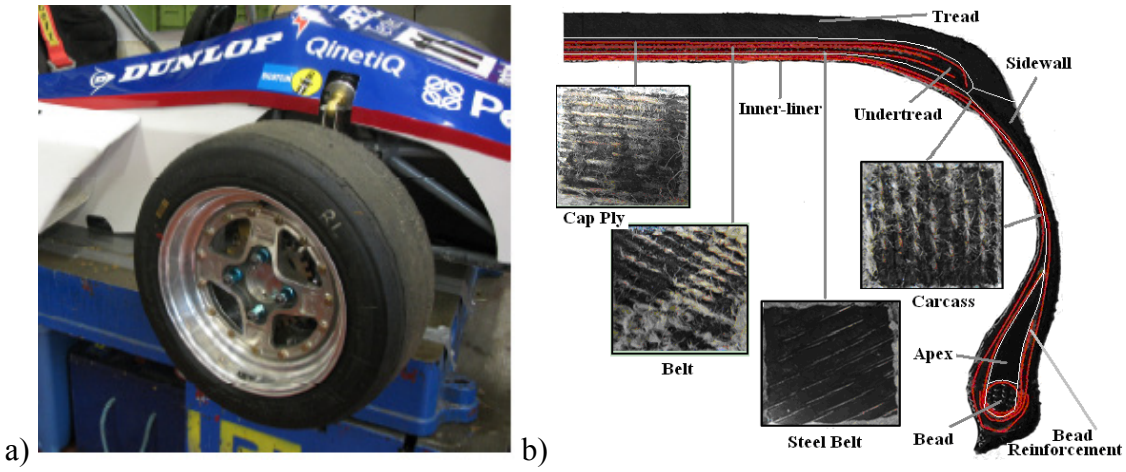

Fig. 1. (a) Formula Student Car with Dunlop Slick Tyre; (b) Cross-section of Dunlop 175/505 R13 Radial Tire.

The pneumatic tire has been equipped with strain gauges on its inner liner [28]. In particular, the KYOWA KFEL-2-120-D35L1M2S high-elongation foil strain gauges have been adopted. These strain gauges are designed for large strain measurement.

Fig. 2 shows the tri-axial arrangement of each set of strain gauges attached to the inner liner of the tire and the positon of the two rectangular rosette strain sensors, mounted symmetrically about the tire tread centre line. The location of the strain gauges has been optimized not only for straight line conditions but also in order to improve the achieved information under cornering conditions [17]. The strain data registered at both sides of the contact patch, symmetrically located about the tire tread centre line, provides crucial information for slip angle estimation.

The deformation behaviour of the inner liner is dominated by the tire carcass; consequently, due to the high value of the carcass stiffness, no local stiffening effect caused by the strain gauges has been considered.

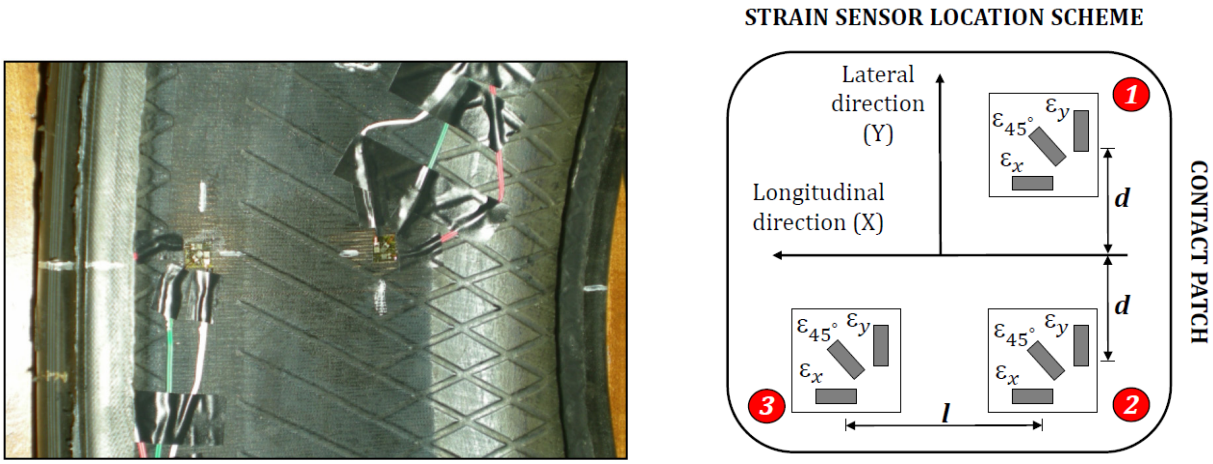

Fig. 2. Arrangements of strain sensors.

The interference with the sensors during the assembly procedure has been avoided by using a rim divided in two pieces (see Fig. 3a). Sealed valves have been used in order to connect the sensors placed inside the tire with the external acquisition system without air flowing (Fig. 3b).

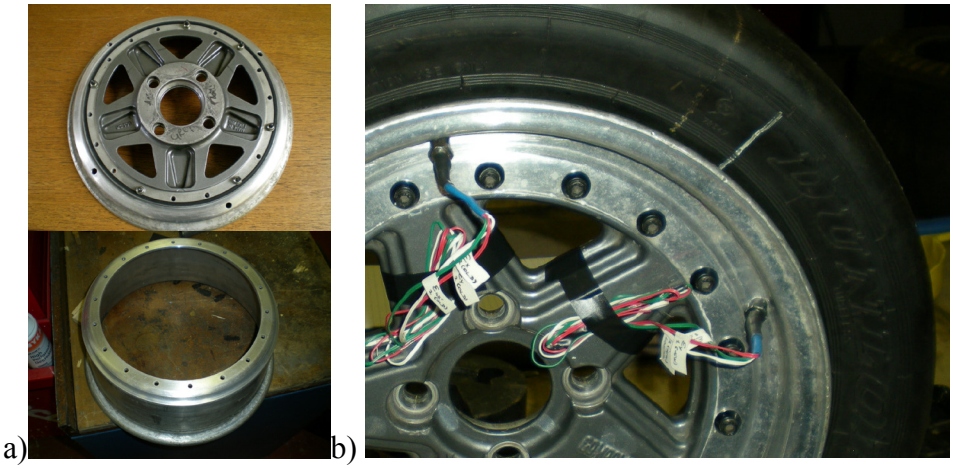

Fig. 3. a) Split Wheel; b) Sealed valves.

The SoMat 2000 Field Computer has been utilized for the test data collection. The adopted system is portable and based on microprocessor data acquisition. The sampling frequency has been fixed at 1000 Hz which can record at least 50 data points per tyre revolution at speed 100 km/h. The measurement range of SoMat strain gauge module is from -5000 microstrain to 5000 microstrain, which is suitable for the normal working range of the adopted intelligent tire prototype.

The testing procedure of the intelligent tire will be illustrated in Section 4 together with experimental results and comparisons with the numerical ones provided by the mathematical model illustrated in the next section.

3. Analytical model of the strain distribution

Analytical modelling of tire/road contact provides a fundamental knowledge of the main characteristics of the tire behaviour. Some examples of these types of model are: point contact model, rigid tread band model, fixed and adaptive footprint models and the flexible ring model [29]. The last one has been widely adopted for describing the in-plane tire behaviour. More specifically, in low frequency range, the flexible ring tire model (FRTM) can reproduce the tire dynamics, which is similar to that of an elastic ring subjected to external excitation forces [30-32].

The model adopted in this study is the FRTM due to the possibility of obtaining, in a closed form, the mathematical description of the tire inner liner circumferential strains. In the FRTM, the treadband structure is modelled as a thin circular elastic ring connected to the wheel hub in circumferential and radial directions through a viscoelastic foundation. The viscoelastic foundation is schematically represented by spring damper elements in the radial and tangential directions. The spring elements have the function of describing the stiffness of the sidewall structure and the membrane stiffness of the inflated torus enclosed by the carcass.

The tangential and radial flexibility of the tread rubber elements of the tire are modelled with another elastic foundation connected to the outside of the elastic ring (schematically represented by the parameters k_{EI} and k_{Gt} in Fig. 4).

A similar modelling approach applied to an intelligent tire is presented in [33], with the main focus on the tire parameter identification from strain measurements. However, the goals of the present paper and of [33] are different. In [33], the contact problem has been solved based on the combination of strain gage measurements, finite element modelling (FEM) and the flexible ring model. Consequently, the research in [33] is focused on parameter identification with computational costs that surely are not compatible with real-time applications. Moreover, in [33], the flexible ring model is that one proposed by Kim *et. al.* [34] which scheme comprises a circular flexible beam and series of radial springs. Compared with the general flexible ring model prosed in this paper, the model in [33, 34] is limited to analyze the tire behavior subjected to only radial forces. In addition, damping effects of sidewall and tangential stiffness of sidewall are neglected in [33, 34]. On the contrary, the real-time physical model presented in this paper, and adopted to reproduce circumferential strain measurements of the tire inner liner, comprises radial and tangential stiffness, damping effects and both radial and tangential forces.

In this analysis, the tire rolling on a flat road at a constant forward speed has been considered. Consequently, the physical problem can be viewed as a stationary tire in rolling contact with a flat road uniformly translating in the opposite direction. In this situation, the rim is fixed in the space and the wheel can only rotate at a constant speed. Fig. 4 shows a scheme of the FRTM.

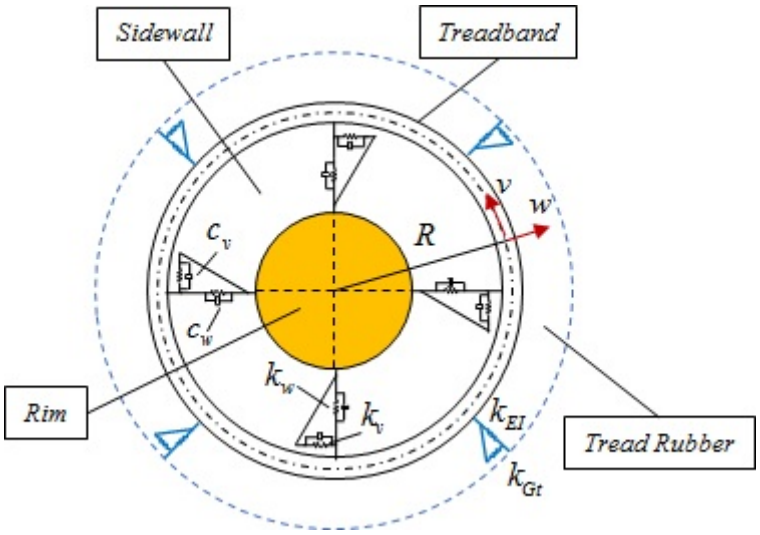

Fig. 4. The flexible ring model.

In Fig. 5, a space-fixed coordinate system and a rotating coordinate system have been defined in order to describe the motion of the FRTM. The main reason for this assumption is that forces and contact deformations can be more conveniently analyzed in a coordinate system which translates with the contact patch, while a coordinate system which rotates with the wheel can be more suitable for describing the dynamics of the rotating treadband.

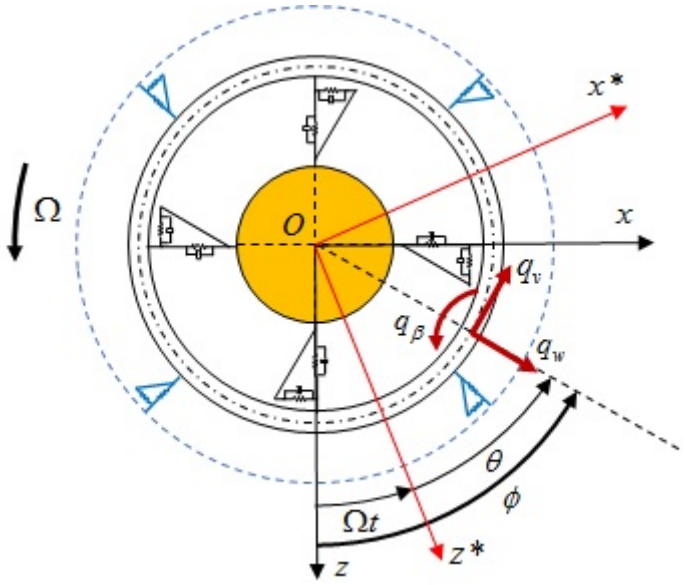

Fig. 5. Coordinate systems.

The origins of both coordinate systems are located at the center of the wheel. The translational displacement of wheel center is described with coordinates (*x, z*) in the non-rotating coordinate system, or (*x*, z**) in the rotating coordinate system. The location of an infinitesimal element of the ring is described in terms of cylindrical coordinates (*r,* ϕ) in the non-rotating coordinate system, or (*r,* θ) in the rotating coordinate system, as shown in Fig. 5. The mathematical transformation between the two coordinate systems is:

$$\begin{aligned} x &= x*\cos(\Omega t) - z*\sin(\Omega t) \\ z &= x*\sin(\Omega t) + z*\cos(\Omega t) \\ \phi &= \theta + \Omega t \end{aligned} \quad , \tag{1}$$

where *t* is the time and Ω is the wheel rotational speed.

According to the Bernoulli-Euler assumption, the treadband has been assumed as an inextensible, curved, bending beam. The introduction of inextensibility assumption is usually valid for rings with high extensional stiffness, which is the case with the most widely used tires. The radial deformation *w* and the tangential deformation *v* at any point on the elastic ring middle surface are related by the following mathematical relation:

$$w = -\frac{\partial v}{\partial \theta}. \tag{2}$$

The rotational angle β of the treadband cross section is defined as:

$$\beta = \frac{1}{R}\left(v - \frac{\partial w}{\partial \theta}\right). \tag{3}$$

The equations of motion of the wheel and the treadband, expressed in terms of *v,* in the rotating coordinate system are [27]:

$$-\frac{EI}{R^4}\left(\frac{\partial^2 v}{\partial\theta^2}+2\frac{\partial^4 v}{\partial\theta^4}+\frac{\partial^6 v}{\partial\theta^6}\right)+\frac{\sigma_\theta^0 A}{R^2}\left(v+2\frac{\partial^2 v}{\partial\theta^2}+\frac{\partial^4 v}{\partial\theta^4}\right)-\frac{p_0 b}{R}\left(v+\frac{\partial^2 v}{\partial\theta^2}\right)-k_w\frac{\partial^2 v}{\partial\theta^2}+k_v\left(v-R\theta_r\right)+$$
$$-c_w\frac{\partial^2\dot{v}}{\partial\theta^2}+c_v\dot{v}+\rho A\left(\ddot{v}-\frac{\partial^2\ddot{v}}{\partial\theta^2}-4\Omega\frac{\partial\dot{v}}{\partial\theta}+\Omega^2\left(\frac{\partial^2 v}{\partial\theta^2}-v\right)\right)=q_v+\frac{\partial q_w}{\partial\theta}+\frac{1}{R}\left(q_\beta+\frac{\partial^2 q_\beta}{\partial\theta^2}\right)$$

$$2\pi k_v R^3\theta_r-R^2\int_0^{2\pi}k_v v\,d\theta=T \tag{4}$$

$$R\int_0^{2\pi}\left(k_w\frac{\partial v}{\partial\theta}\cos\theta-k_v v\sin\theta\right)d\theta=F_{x^*}$$

$$R\int_0^{2\pi}\left(k_w\frac{\partial v}{\partial\theta}\sin\theta+k_v v\cos\theta\right)d\theta=F_{z^*}$$

where dot (·) denotes differentiation with respect to time; T is the torque acting on the rim, F_{x^*} and F_{z^*} are external forces acting at the rim center described in the rotating coordinate system; q_v, q_w and q_β are the external forces in the tangential and radial directions and the moment acting on the ring, respectively; θ_r is a small deviation of the angular displacement of the rim which may be described as a windup rotation resulting from the application of a torque; σ_θ^0 is the initial stress in the treadband due to the action of the centrifugal force and inflation pressure p_0. In particular, the effects of the pressurized air in the FRTM are introduced in two ways: a) the stiffness of the tangential and radial springs are considered to vary with the inflation pressure of the tire; and b) the circular ring is pre-stressed by the inflation pressure and centrifugal forces due to rotation [27].

The relation between σ_θ^0 and the rotating speed Ω and the inflation pressure p_0 of the tire is determined by the following equation:

$$\sigma_\theta^0 A=\left(p_0 bR+\rho AR^2\Omega^2\right) \tag{5}$$

The parameters of Eqs. (4) and (5) are listed in Tab. 1;

Symbol	Description	Unit
b	Width of the ring.	m
h	Thickness of the ring.	m
A	Area of the cross section of the ring ($A=bh$).	m^2
E	Young's modulus of the ring material.	N/m^2
I	Inertia moment of the cross-section of the ring ($I=bh^3/12$).	m^4
R	Mean radius of the ring (tire treadband).	m
ρ	Density of the ring material.	kg/m^3
k_w, k_v	Stiffness of the viscoelastic foundation per unit length in the radial and tangential directions, respectively.	N/m^2
c_w, c_v	Damping of the viscoelastic foundation per unit length in the radial and tangential directions, respectively.	$N\ s/m^2$

Table 1. Parameters of the FRTM.

The solution of (4) has been obtained by adopting the *Modal Expansion Method* (MEM). The fundamental assumption of the MEM is that the response of a linear system to any external excitation forces can be expressed as a weighted summation of the natural mode shapes of the system. The mode shapes of a system are usually time independent while the weight factors are space independent. Adopting the mode shapes of the FRTM, the sixth order partial differential equation of motion of the treadband (see Eqs. (4) for reference) reduces to a set of second order ordinary differential equations in time [27, 35]. According to the MEM, the tangential and radial displacements of the ring, in the rotating coordinate system, can be expressed as follows:

$$\begin{aligned} v(\theta,t) &= \sum_{n=0}^{\infty}\left[a_n(t)\cos(n\theta)+b_n(t)\sin(n\theta)\right] \\ w(\theta,t) &= -\frac{\partial v}{\partial \theta} = \sum_{n=0}^{\infty}\left[n a_n(t)\sin(n\theta)-n b_n(t)\cos(n\theta)\right] \end{aligned} \tag{6}$$

where n denotes the mode number and $a_n(t)$ and $b_n(t)$ are the generalized modal displacement. In the present study, the moment acting on the ring has been neglected ($q_\beta = 0$). In this case, the external line forces on the ring are

$$\begin{aligned} q_w(\theta,t) &= Q_w\delta(\phi-\phi_0) = Q_w\delta(\theta-(\phi_0-\Omega t)) \\ q_v(\theta,t) &= Q_v\delta(\phi-\phi_0) = Q_v\delta(\theta-(\phi_0-\Omega t)) \end{aligned} \tag{7}$$

where Q_w and Q_v are the magnitudes of radial and tangential line forces acting at specified stationary angular coordinate ϕ_0, in the non-rotating coordinates or the corresponding point, $(\theta - \theta_0)$, where $(\theta_0 = \phi_0 - \Omega t)$ in the rotating coordinates; $\delta(\theta - (\phi_0 - \Omega t))$ is a Dirac delta function. The steady state response of the FRTM in terms of the tangential displacement and the corresponding radial displacement of the tire treadband for the concentrated line forces are given by [35]:

$$v(\phi) = \sum_{n=0}^{\infty} \left[A_{n1} Q_v \cos n(\phi_0 - \phi + \gamma_n) + A_{n2} Q_w \sin n(\phi_0 - \phi + \gamma_n) \right] \tag{8}$$

where

$$A_{n1} = \frac{1}{\pi \sqrt{(M_n - G_n)^2 + (C_n)^2}}$$

$$A_{n2} = n A_{n1}$$

$$n\gamma_n = \tan^{-1}\left(\frac{C_n}{M_n - G_n} \right)$$

$$M_n = k_n - (n\Omega)^2 m_n$$

$$G_n = (n\Omega) g_n$$

$$C_n = (n\Omega) c_n$$

$$m_n = \rho A (1 + n^2)$$

$$g_n = -4 \rho A n \Omega$$

$$c_n = c_v + c_w n^2 \tag{9}$$

$$k_n = \left(\frac{EI}{R^4} n^2 + \frac{\sigma_\theta^0}{R^2} \right)(1 - n^2)^2 - \frac{p_0 b}{R}(1 - n^2) + k_v + k_w n^2 - \rho A (1 + n^2) \Omega^2$$

The solution of the FRTM for a distributed vertical load could be obtained with the superimposition principle. Consider a distributed load extending from the angular coordinate ϕ_f at the front edge of the contact patch to ϕ_r at the rear edge can be applied to the tire. The normal pressure distribution acting on the contact patch could be modelled with a parabolic function of the angular coordinate as follows:

$$q_z(\phi) = \frac{3}{4}\frac{F_z}{R\phi_r^3}\left(\phi_r^2 - \phi^2\right), \tag{10}$$

where F_z is the vertical load acting on the wheel and the symmetrical condition $\phi_r = -\phi_f$ is considered.

The corresponding radial pressure distribution can be obtained as:

$$q_w(\phi) = \frac{3}{4}\frac{F_z}{R\phi_r^3}\left(\phi_r^2 - \phi^2\right)\cdot\frac{1}{\cos(\phi)}. \tag{11}$$

By dividing the extension of the contact patch in N_ϕ constant angular steps $\Delta\phi$, the generic concentrated forces $Q_{w,i}$ and $Q_{v,i}$ acting at point, with angular coordinate $\phi_{0,i}$, can be written as:

$$\begin{aligned} Q_{w,i} &= q_w\left(\phi_{0,i}\right)\Delta\phi \\ Q_{v,i} &= q_v\left(\phi_{0,i}\right)\Delta\phi \end{aligned}. \tag{12}$$

Hence, the tangential and radial deformations can be obtained by superimposing the solution:

$$\begin{aligned} v(\phi) &= \sum_{i=1}^{N_\phi}\sum_{n=0}^{\infty}\left[A_{n1}Q_{v,i}\cos\left(n\left(\phi_{0,i} - \phi + \gamma_n\right)\right) + A_{n2}Q_{w,i}\sin\left(n\left(\phi_{0,i} - \phi + \gamma_n\right)\right)\right] \\ w(\phi) &= \sum_{i=1}^{N_\phi}\sum_{n=0}^{\infty} n\left[-A_{n1}Q_{v,i}\sin\left(n\left(\phi_{0,i} - \phi + \gamma_n\right)\right) + A_{n2}Q_{w,i}\cos\left(n\left(\phi_{0,i} - \phi + \gamma_n\right)\right)\right] \end{aligned}, \tag{13}$$

Finally, the strain in the circumferential direction of the treadband [15, 27], can be expressed as:

$$\varepsilon_\theta = \frac{y}{R^2}\left(\frac{\partial v}{\partial\theta} - \frac{\partial^2 w}{\partial\theta^2}\right), \tag{14}$$

in which y is the distance from the treadband middle surface.

Substituting equations (13) into (14), the circumferential strain can be obtained as follows:

$$\varepsilon_\theta(\phi)=\sum_{i=1}^{N_\phi}\sum_{n=1}^{\infty}\frac{y}{R^2}n^3\left[A_{n1}Q_{v,i}\sin\left(n\left(\phi_{0,i}-\phi+\gamma_n\right)\right)-A_{n2}Q_{w,i}\cos\left(n\left(\phi_{0,i}-\phi+\gamma_n\right)\right)\right]. \quad (15)$$

The mathematical relation (15) represents a closed form solution of the FRTM in terms of circumferential treadband strains. The numerical model outputs have been compared with the measurements provided by the adopted intelligent tire. The carcass deformations have been obtained taking into account distributed loads acting on the contact patch.

4. Experimental model validation

The test system used for the experiments is an indoor tire test rig which makes it possible to vary speed, vertical load and slip angle. The tire test rig also allows to simulate different surface types by installing rough sheets on the drum. The experiment setup is shown in Fig. 6.

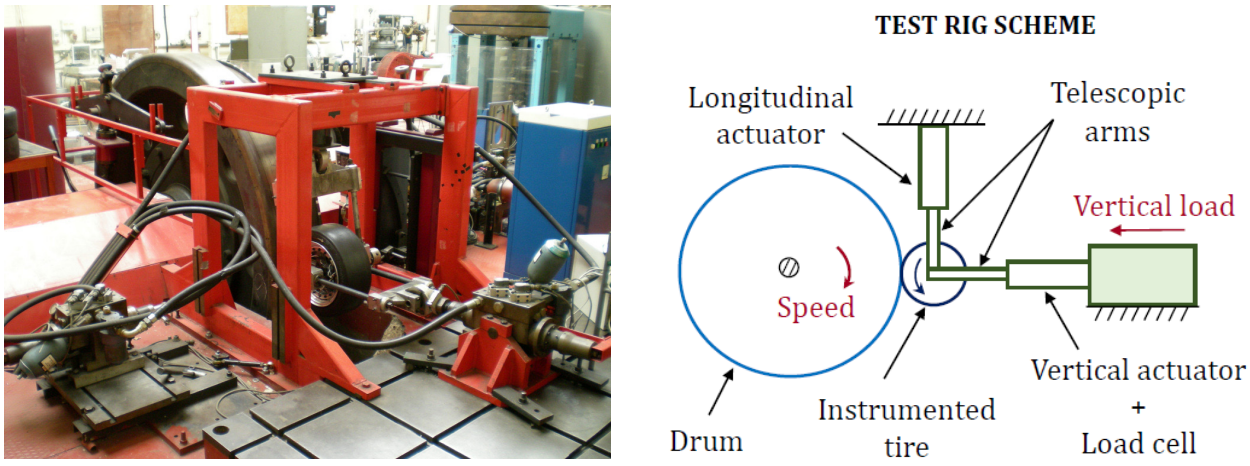

Fig. 6. Test rig.

The experiments have been carried out in straight rolling condition. The influence of the tire operative conditions (tire rolling speed, inflation pressure and vertical load) on the strain measurements have been deeply analysed in previous works [1, 17, 28].

The indoor test rig allows the variation of operative conditions without stopping the intelligent tire prototype. For instance, Fig. 7 shows the transition period while vertical load is being changed.

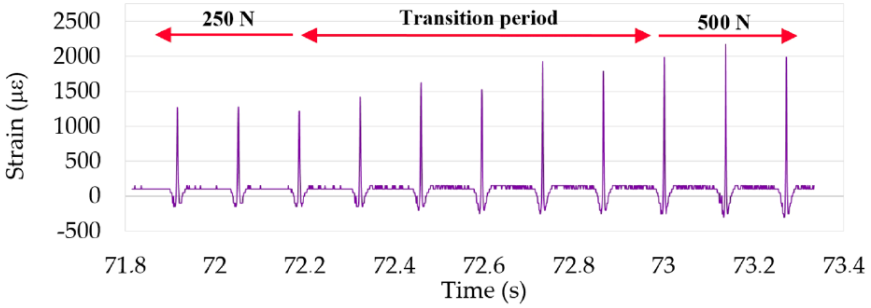

Fig. 7. Circumferential strains for different vertical loads [1].

In the study, the main goal is the validation of a real-time FRTM capable of reproducing the strain measurements provided by the intelligent tire for in-plane motions. The experimental data selected for the model validation are only the circumferential strains. The results have been obtained with the tire in straight-line free rolling conditions. In particular, the influence of the tire speed and the vertical load has been evaluated. The operative tire conditions used for the tests are listed below:

Tire inflation pressure: 1 bar;
Tire vertical load: 250 N–1000 N;
Tire speed: 10 km/h–50 km/h;
Tire slip angle: 0;

An identification procedure has been performed by varying the model parameters and minimizing the error between the measured strains with the numerical ones. The identified FRTM parameters are listed in Tab. 2.

Parameters	Value	Unit
b	0.175	m
h	0.002	m
EI	0.03	Nm^2
R	0.23	m
ρ	2000	kg/m^3
k_w	500000	N/m^2
k_v	100000	N/m^2
$c_w = c_v$	0	$N\ s/m^2$

Table 2. Values of the identified FRTM parameters.

Fig. 8 and Fig. 9 show the comparison between experimental and numerical results for the same tire velocity (10 km/h) and vertical load equal to 250 N and 500 N, respectively.

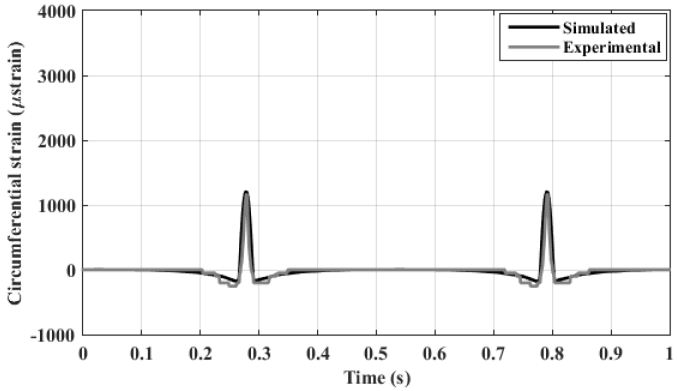

Fig. 8. Circumferential strain (velocity: 10 km/h; vertical load: 250 N).

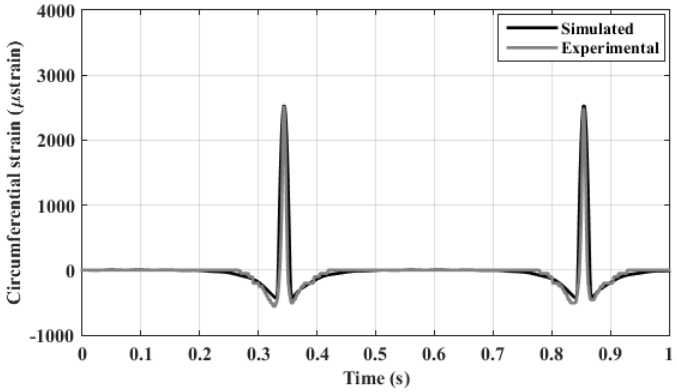

Fig. 9. Circumferential strain (velocity: 10 km/h; vertical load: 500 N).

The simulated strains for both vertical loads provide a good matching with the experimental results. The simulated treadband vertical displacements for both vertical loads are reported in Figs. 10a 10b.

a)

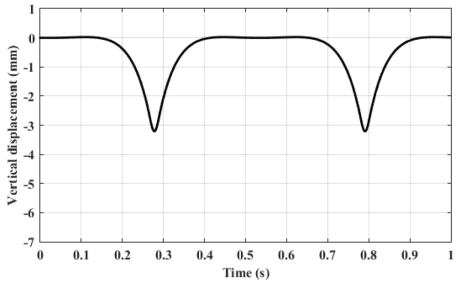

b)

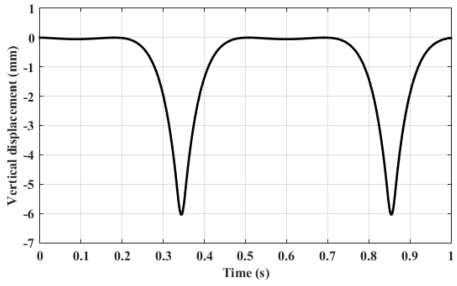

Fig.10. Treadband vertical displacement (velocity: 10 km/h); a) vertical load: 250 N; b) vertical load: 500 N.

The values of vertical displacements shown in Figs. 10a,b are in accordance with previous experimental studies [28] oriented to measure the behaviour of the intelligent tire prototype under static vertical loads (see Fig. 11 for reference).

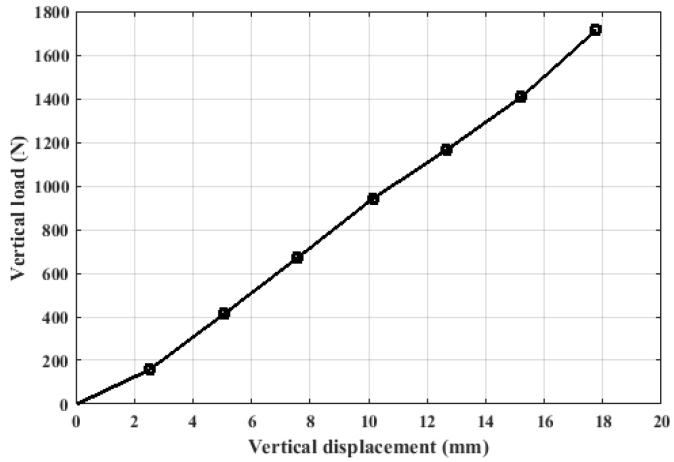

Fig. 11. Experimental vertical displacement/load at 100 kPa inflation pressure.

Another comparison has been performed in order to evaluate the effect of the tire rotational velocity on the measured strain. Fig. 12 and Fig. 13 show the comparison between the model outputs and the experimental data for the same vertical load (250 N) and velocities equal to 20 km/h and 30 km/h, respectively.

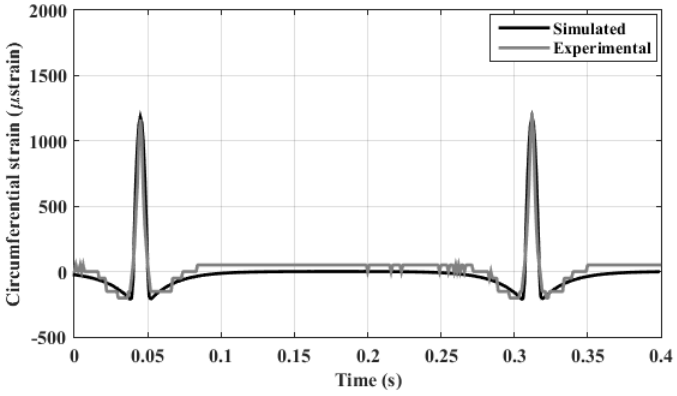

Fig. 12. Circumferential strain (velocity: 20 km/h; vertical load: 250 N).

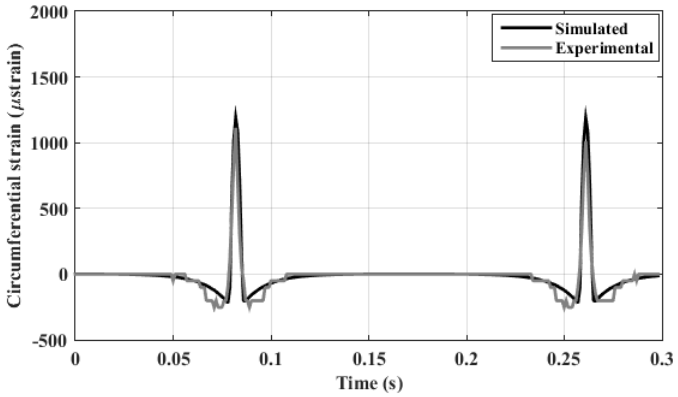

Fig. 13. Circumferential strain (velocity: 30 km/h; vertical load: 250 N).

Also for these tests, the model is able to track the main behaviour of the measured strains.

A comparison between simulated and measured strains have been executed for higher values of vertical load (750 N) and velocity (50 km/h). Fig. 14 and Fig. 15 show the circumferential strains and the carcass shape before and after compression, respectively.

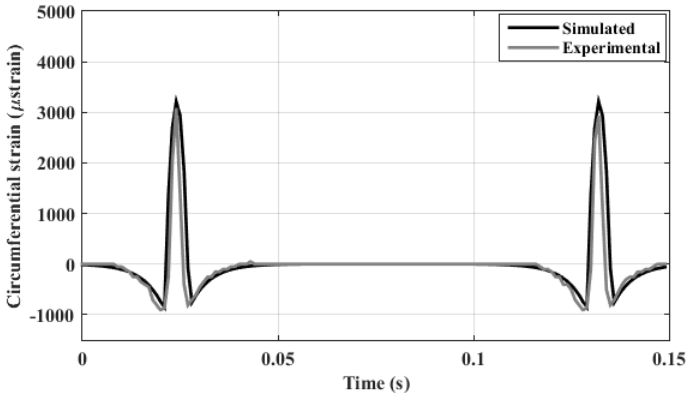

Fig. 14. Circumferential strain (velocity: 50 km/h; Vertical load: 750 N).

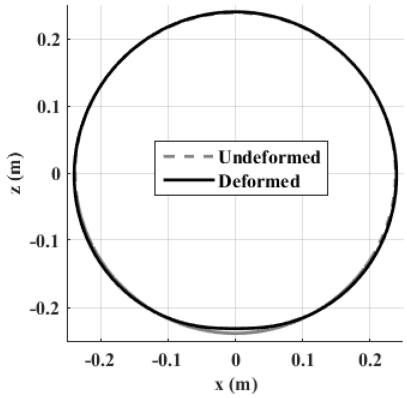

Fig. 15. Simulated tire carcass contours from the FRTM (velocity: 50 km/h; vertical load: 750 N).

Model outputs are in good accordance with the experimental results and the estimated tire deformed shape can be considered reliable.

It is important to note that the most accurate way to analyse the influence of the load in the strain data is obtained by means of the variation of the compressive peaks in circumferential strains [1]. Fig. 16 shows the trend of the simulated and experimental strain compressive peaks with respect to the vertical loads.

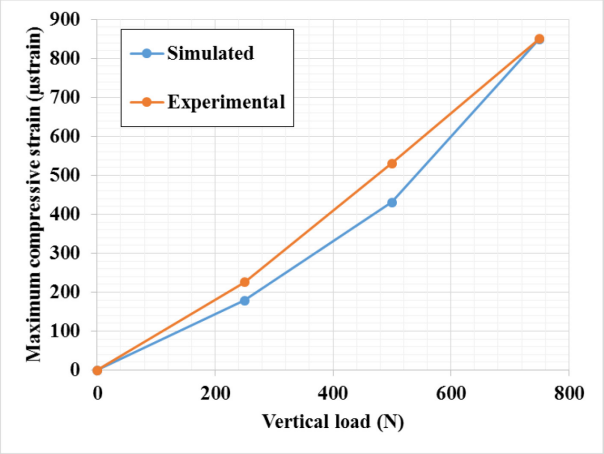

Fig. 16. Maximum compressive strain (absolute value).

Results of Fig. 16 clearly highlight a similar variation of the numerical and experimental strain compressive peaks in function of the applied vertical loads. However, some differences between model outputs and measurements still occur. Probably this discordance is due to nonlinearities of the actual tire mechanical structure.

Two further experimental tests have been executed to verify the capability of the proposed FRTM in the case of combined vertical and longitudinal loads. Figs. 17 and 18 show comparisons between experimental and simulated circumferential strains for two different values of the applied longitudinal force: F_x=485 N and F_x=505 N, for the same vertical force F_z=1000 N, and for rolling velocities of 10 km/h and 30 km/h, respectively.

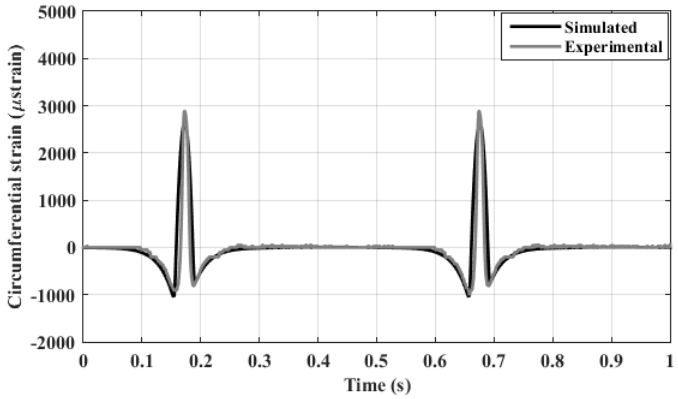

Fig. 17. Circumferential strain (velocity: 10 km/h; vertical load: 1000 N, longitudinal load: 485 N).

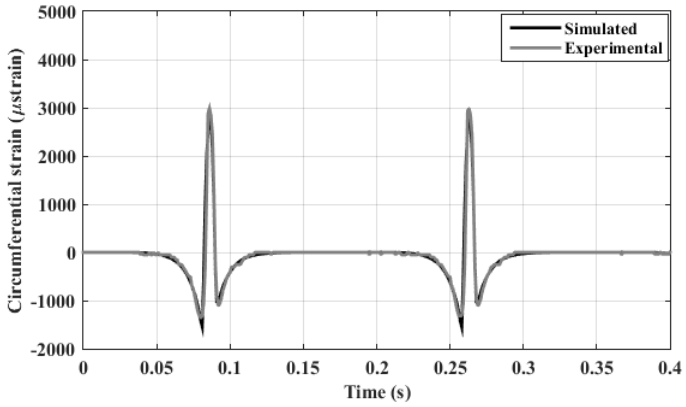

Fig. 18. Circumferential strain (velocity: 30 km/h; vertical load: 1000 N; longitudinal load: 505 N).

Also in this case the FRTM is able to reproduce the trend of measurements characterized by asymmetrical behaviours due to the longitudinal forces acting on the intelligent tire.

5. Conclusions and future developments

An analytical model suitable to describe the behaviour of tire strains has been presented. The tire has been modelled with a flexible ring on a viscoelastic foundation. The radial and tangential displacements of the tire carcass have been obtained in closed form with the modal expansion method. Consequently, the tire inner liner strains have been expressed as functions of the tire carcass deformations. The simulated strains have been obtained by taking into account distributed loads acting on the tire contact patch. The validation of the proposed tire strain model has been performed by adopting a strain-based intelligent tire. An experimental setup has been adopted for indoor tests and correlations between the measured tire strains and the ones provided by the developed physical model have been analysed. Experimental and numerical results have been compared demonstrating the high performance of the proposed modelling approach. In particular, the experimental validation highlighted that the flexible ring model is able to predict the circumferential strains of the tire inner liner in the presence of both vertical and longitudinal forces. The presented mathematical model could be used for simulations of strain-based intelligent tires.

Moreover, the developed real-time tire flexible ring model could be implemented in the design of observers for tire condition estimations from strain measurements.

References

[1] Garcia-Pozuelo, D., Olatunbosun, O., Yunta, J., Yang, X., Diaz, V. A novel strain-based method to estimate tire conditions using fuzzy logic for intelligent tires (2017) Sensors (Switzerland), 17 (2), art. no. 350.

[2] Kim, S.J., Kim, K.-S., Yoon, Y.-S. Development of a tire model based on an analysis of tire strain obtained by an intelligent tire system (2015) International Journal of Automotive Technology, 16 (5), pp. 865-875.

[3] Lee, H., Taheri, S. Intelligent tires-a review of tire characterization literature (2017) IEEE Intelligent Transportation Systems Magazine, 9 (2), art. no. 7904765, pp. 114-135.

[4] Singh, K.; Bedekar, V.; Taheri, S.; Priya, S. Piezoelectric vibration energy harvesting system with an adaptive frequency tuning mechanism for intelligent tires. Mechatronics 2012, 22, 970–988.

[5] Negrus, E.; Anghelache, G.; Sorohan, S. Tire Radial Vibrations at High Speed of Rolling; SAE: Detroit, MI, USA, 1998.

[6] Hong, S.; Erdogan, G.; Hedrick, K.; Borrelli, F. Tyre–road friction coefficient estimation based on tyre sensorsand lateral tyre deflection: Modelling, simulations and experiments. Veh. Syst. Dyn. 2013, 51, 627–647.

[7] F. Braghin, M. Brusarosco, F. Cheli, A. Cigada, S. Manzoni, and F. Mancosu, “Measurement of contact forces and patch features by means of accelerometers fixed inside the tire to improve future car active control,” Vehicle Syst. Dyn., vol. 44, no. 1, pp. 3–13, Jan. 2006.

[8] APOLLO Consortium, “Final report including technical implementation plan (annex),” Technical Research Centre of Finland (VTT), APOLLO Deliverable 22/23 for Project IST-2001-34372, 2005.

[9] K. S. Moona, H. Liangb, J. Yi, and B. Mika, “Tire tread deformation sensor and energy harvester development for “Smart Tire” applications,” in Proc. Sensors and Smart Structures Technologies for Civil, Mechanical, and Aerospace System, San Diego, CA, 2007.

[10] J. Yi, “A piezo-sensor-based ‘smart tire’ system for mobile robots and vehicles,” IEEE/ASME Trans. Mechatron., vol. 13, no. 1, pp. 95–103, Feb. 2008.

[11] A. Pohl, R. Steindl, and L. Reindl, “The ‘intelligent tire’ utilizing passive SAW sensors measurement of tire friction,” IEEE Trans. Instrum. Meas., vol. 48, no. 6, pp. 1041–1046, 1999.

[12] A. Todoroki, S. Miyatani, and Y. Shimamura, “Wireless strain monitoring using electrical capacitance change of tire: Part I—with oscillating circuit,” Smart Mater. Struct., vol. 12, no. 3, pp. 403–409, May 2003.

[13] O. Yilmazoglu, M. Brandt, J. Sigmund, E. Genc, and H. L. Hartnagel, “Integrated InAs/GaSb 3D magnetic field sensors for ‘the intelligent tire,” Sens. Actuators A, vol. 94, no. 1/2, pp. 59–63, Oct. 2001.

[14] A. Miyoshi, T. Tsurita, and M. Kunni, “System and method for determining tire force,” U.S. Patent 7 249 498, July 31, 2007.

[15] N. Roveri, G. Pepe, A. Carcaterra, “OPTYRE – A new technology for tire monitoring: Evidence of contact patch phenomena,” Mechanical Systems and Signal Processing, vol. 66–67, pp. 793-810, 2016.

[16] Breglio, G., Fienga, F., Irace, A., Russo, M., Strano, S., Terzo, M. Fiber Bragg gratings for strain and temperature measurements in a smart tire (2017) Lecture Notes in Engineering and Computer Science, 2230, pp. 759-763.

[17] Garcia-Pozuelo, D., Yunta, J., Olatunbosun, O., Yang, X., Diaz, V. A strain-based method to estimate slip angle and tire working conditions for intelligent tires using fuzzy logic (2017) Sensors (Switzerland), 17 (4), art. no. 874.

[18] Canudas de Wit, C. and Tsiotras, P. (1999). Dynamic tire friction models for vehicle traction control. Proc. 38th Conf. Decision & Control, 4, 3746−3751.

[19] Tonuk, E. and Unlusoy, Y. S. (2001). Prediction of automobile tire cornering force characteristics by finite element modeling and analysis. Computers & Structure 79, 13, 1219−1232.

[20] Lee, C. R., Kim, J. W., Hallquist, J. O., Zhang, Y. and Farahani, A. D. (1997). Validation of a FEA tire model for vehicle dynamic analysis and full vehicle real time proving ground simulations. SAE Paper No. 971100.

[21] Holtschulze, J., Goertz, H. and Husemann, T. (2005). A simplified tyre model for intelligent tyres. Vehicle System Dynamics, 43, 305−316.

[22] Rajamani, R. (2012). Vehicle Dynamics and Control. 2nd edn. Springer. New York.

[23] Jazar, R. N. (2008). Vehicle Dynamics: Theory and Application. Springer. New York.

[24] Pacejka, H. B. and Bakker, E. (1992). The magic formula tyre model. Int. J. Vehicle Mechanics and Mobility 21, 1, 1−18.

[25] Pacejka, H. B. (2005). Tire and Vehicle Dynamics. 2nd edn. Butterwoth-Heinemann. London.

[26] Yang, X.; Olatunbosun, O.; Garcia-Pozuelo Ramos, D.; Bolarinwa, E. FE-Based Tire Loading Estimation for Developing Strain-Based Intelligent Tire System; SAE: Detroit, MI, USA, 2015.

[27] S. Gong, A Study of In-Plane Dynamics of Tires, Delft University, 1993.

[28] Yang X. Finite element analysis and experimental investigation of tyre characteristics for developing strain-based intelligent tyre system. In Mechanical engineering. Birmingham: University of Birmingham; 2009.

[29] P.W.A. Zegelaar, The dynamic response of tyres to brake torque variations and road unevennesses, Ph.D. thesis, Delft University of Technology, 1998.

[30] Xiong, Y., Tuononen, A. The in-plane deformation of a tire carcass: Analysis and measurement (2015) Case Studies in Mechanical Systems and Signal Processing, 2, pp. 12-18.

[31] P. Kindt, P. Sas, W. Desmet, Development and validation of a three-dimensional ring-based structural tyre model, J. Sound Vib. 326 (2009) 852–869,

[32] C. Hoever, The Simulation of Car and Truck Tyre Vibrations, Rolling Resistance and Rolling Noise, Chalmers University of Technology, 2014.

[33] Lee, H., & Taheri, S. (2018). A novel approach to tire parameter identification. Proceedings of the Institution of Mechanical Engineers, Part D: Journal of Automobile Engineering, 0954407018771253.

[34] Kim S. A comprehensive analytical model for pneumatic tires. Tucson, AZ: The University of Arizona, 2002.

[35] Kim, Son-Joo, Savkoor, Arvin R. Contact problem of in-plane rolling of tires on a flat road (1997) Vehicle System Dynamics, 27 (Suppl), 345 p.